Microporous and Mesoporous Materials 142 (2011) 130–138

Contents lists available at ScienceDirect

Microporous and Mesoporous Materials

journal homepage: www.elsevier.com/locate/micromeso

Preparation and characterization of nano-silver/mesoporous titania photocatalysts for herbicide degradation

Mohamed Mokhtar Mohamed *,[1], K.S. Khairou

Umm Al Qura University, Faulty of Applied Science, Chemistry Department, Saudi Arabia

ARTICLE INFO

Article history:
Received 29 August 2010
Received in revised form 17 November 2010
Accepted 18 November 2010
Available online 25 November 2010

Keywords:
Mesoporous titania
Ag nanoparticles
Template self assembly
Characterization
Photocatalysis

ABSTRACT

Hydrothermally synthesized mesoporous titania containing silver; at weight percentages ratio of 1.6 and 3.2, nanoparticles either assembled by polyoxyethylene laurel ether (POL) or sodium dodecylsulphate (SDS) were characterized with XRD, N_2 sorptiometry, DRUV–vis, FTIR and TEM. The photocatalytic performance of the catalysts was tested for the oxidation of 2,4-dichlorophenoxyacetic acid (2,4-D; herbicide); through comparison with P25, under visible ($\lambda > 420$ nm) and UV light irradiation. Our results show that TEM measurements evince that dispersed Ag nanoparticles with diameter of 7 and 5 nm are deposited on titania surfaces synthesized using POL and SDS, respectively. XRD and N_2 sorptiometry measurements advocate that Ag atoms were present inside titania pores; as confirmed from decreasing both surface area and pore volume values, as well as attending on titania surfaces upon increasing Ag content prohibiting the growth of anatase phase. The UV–vis absorbance spectra indicated that Ag nanoparticles can shift the absorption maximum to the visible light region as confirmed by the presence of surface plasmon bands at 634 and 700 nm. The apparent rate constants calculated under visible-light illumination for all catalysts were 0.0335 and 0.0289 min^{-1}; for 1.6 wt.% and 3.2 wt.% Ag/TiO_2 templated from POL, as well as 0.0263 and 0.0251 min^{-1}; for 1.6 wt.% and 3.2 wt.% Ag/TiO_2 templated from SDS. The direct involvement of the Ag particles in mediating the electron transfer from the photoexcited TiO_2 under band gap excitation is considered to carry out the efficient photo-catalytic oxidation of the 2,4-D besides, the higher efficiency of generation, mobility, and separation of photoinduced electrons and holes.

© 2010 Elsevier Inc. All rights reserved.

1. Introduction

The chemistry of titania has been studied for many years as results of its interesting photocatalytic properties [1,2]. For example, titania has been used to mediate the photo-catalytic oxidation of aromatic compounds [1,2] and the photochemical splitting of water [3]. Recently, there has been a great deal of interest in the synthesis of nanostructured titania [4–6], in an effort to increase the efficiency of these photochemical processes. In addition, a variety of attempts has been made to introduce various metal species into the TiO_2 matrix in an effort to enhance the photocatalytic activity and/or broaden the absorption of the solar spectrum by the doped TiO_2. Methods that have been used include ion exchange, impregnation and co-precipitation [7,8]. Some interesting effects have been observed from these implantation studies. Metal-doped TiO_2 has been widely studied for improving photocatalytic performance on the degradation of various organic pollutants under visible-light irradiation [9–11]. Ag doping directly influences the intrinsic properties of TiO_2, such as charge carried recombination rates, the particle size and interfacial electron-transfer rates and extending photoresponse of TiO_2 into the visible range [12–14]. The noble metal which acts as a sink for photo-induced charge carriers, promotes interfacial charge-transfer processes. Additionally, recent investigations on gold titania nanocomposite particles also show that the presence of nanosized gold particles supported on TiO_2 extended the response of the photocatalyst into visible light region due to defects associated with oxygen vacancies that give rise to color centers displaying the absorption bands [15,16].

Herbicides are a class of pesticides that are marketed specifically for the purpose of killing or inhibiting the growth of weeds. The benefits of herbicide use have been many. In agriculture, herbicides control weeds that may rob water and nutrients from crop plants [17]. Compared to other methods, like tillage, herbicides have been promoted as methods of weed control that lessen the impact of soil erosion. They have also been used to control aquatic weeds that block water intakes or invade natural ecosystems, as well as in forestry, and even in swimming pools to inhibit growth of algae [18]. These benefits have resulted in a steady demand for pesticides to be in use all over the world. However, almost all herbicides can cause acute toxicity. Phenoxy herbicides are one of the

* Corresponding author. Tel.: +966 500969808.
E-mail address: mohmok2000@yahoo.com (M.M. Mohamed).
[1] Permanent address: Benha University, Faculty of Science, Chemistry Department, Benha, Egypt

1387-1811/$ - see front matter © 2010 Elsevier Inc. All rights reserved.
doi:10.1016/j.micromeso.2010.11.026

most widely used and thus involved in acute symptomatic illnesses associated with a variety of chronic health risks. Most notable have been concerns about carcinogenicity. Pesticides have the potential to cause adverse effects on humans, wildlife, fish, or plants, including endangered species and non-target organisms, as well as possible contamination of surface water or groundwater from leaching, runoff, and spray drift [19]. Herein, we report facile synthesis methods for mesoporous TiO_2 nanoarchitectures containing silver and their application as photocatalysts for degradation of the herbicide 2,4-dichlorophenoxyacetic acid under both UV–vis and visible irradiation.

2. Experimental

2.1. Materials synthesis

The mesoporous TiO_2 samples were synthesized as follows:

An aqueous solution of polyoxyethylene laurel ether (POL) template was prepared by dissolving with a mixture of ethanol and water, and then mixed with the desired ratio of $AgNO_3$ solutions. A drop wise addition of Titanium iso-propoxide into the previous mixture was accomplished that lasts for two hours till complete hydrolysis. The molar ratio of the mixture was Ti:Ag:H_2O:ETOH: template = 1:0.1–0.2:12–14:34:0.012. The resulting emulsion solutions were mixed thoroughly for further 2 h and then aged for 5 h at ambient temperature. They were transformed into autoclaves lined with Teflon and followed by hydrothermal treatment at 373 K for 24 h for each mixture. After hydrothermal treatment, the products were recovered by centrifugation and then washed three times with deionized water. The solids were then isolated by filtrations and washed once again with deionized water and dried overnight at 333 K. They further calcined in air at 723 K for 4 h to remove the template. The samples were denoted as A and B based on the used template POL and Ag wt.%, where A represents 1.6 wt.% and B represents 3.2 wt.% of $AgNO_3$.

The photocatalyst is also synthesized using a deposition–precipitation method. An aqueous solution of Ti iso-propoxide in isoproponal and silver nitrate with different ratios (1.6 and 3.2 wt.%) were dropped onto sodium dodecyl sulphate (20%) surfactant dissolved in isopropanol and water. Simultaneous additions of suitable amounts of hydrazine (0.5 g of 80% in 150 ml) and ammonium hydroxide (25%) for reduction of Ag^+ ions and depositing it on/in the precipitated Ti^{4+} support, under vigorous stirring, were performed. The products were left for about 2 h. The catalysts were then recovered by filtration and washing with methanol and deionized water and dried at 333 K in air over night. Finally, they are calcined at 723 K for 4 h. The samples were denoted as C and D based on the used silver nitrate weight percentages upon using SDS (1.6 and 3.2 wt.%, respectively). P25 TiO_2 (80% anatase, 20% rutile and S_{BET} = 59 m^2/g) that purchased from Degussa (Germany) was used for comparison purposes.

2.2. Characterization

The X-ray diffractograms of various samples were measured by using a Philips diffractometer (type PW 3710). The patterns were run with Ni-filtered copper radiation (λ = 1.5404 Å) at 30 kV and 10 mA with a scanning speed of $2\theta = 2.5^\circ$ min^{-1}. The instrumental line broadening was measured using a LaB6 standard. FT-IR spectra of the samples were recorded with a JASCO single beam FT-IR 5300-spectrometer with 50 co-added scans at 2 cm^{-1} resolution. All IR measurements were carried out at room temperature using KBr disks. Diffuse reflectance UV–vis spectra of the materials were obtained for the dry pressed disk samples using UV–vis spectrophotometer (Shimadzu 2101-PC) between 200–800 nm range. Absorption spectra were referenced to $BaSO_4$. The nitrogen adsorption isotherms were measured at 77 K using a conventional volumetric apparatus. The specific surface area was obtained using the BET method. The micropore volume and the external surface area were obtained from the t-plot method. TEM micrographs were measured using a Philips, model Tecani Feil2, at an accelerating voltage of 200 kV. The powder samples were put on carbon foil with a microgrid. TEM images were observed with minimum electron irradiation to prevent damage to the sample structure.

2.3. Photocatalytic experiments

The photocatalytic activity of each sample was evaluated in terms of the degradation of 2,4-dichlorophenoxyacetic acid that chosen as a model pollutant. This herbicide solution (50 ppm, 100 ml) is prepared by dissolving the required amount in deionized water by continuous stirring. Prior to the start of light experiments, dark (adsorption) experiments are carried out for 60 min under continuous stirring for better adsorption of the herbicide onto the surface of catalyst (0.15 g). A 300-W tungsten halogen lamp equipped with a UV cut-off filters (l > 365 nm) was used as an ultraviolet light source (the average light intensity was 60 mW cm^{-2}) and a 300-W high-pressure Hg lamp for which the strongest emission wavelength is 420 nm was used as a visible light source (the average light intensity was about 120 mW cm^{-2}). The lamp was cooled with flowing water in a quartz cylindrical jacket around the lamp, and ambient temperature is maintained during the photocatalytic reaction. At the given time intervals, the analytical samples were taken from the mixture and immediately centrifuged, then filtered through a 0.22-mm Millipore filter to remove the photocatalysts. The concentration of the filtrate was analyzed by checking the absorbance at 294 nm with a UV–vis spectrophotometer (Varian Cary 100). The reproducibility was checked by repeating the measurements at least three times and was found to be within the acceptable limit (5%).

3. Results and discussion

3.1. X-ray diffraction

The low angle and wide angle XRD patterns of as-synthesized products are presented in Fig. 1a and 1b, respectively. The low angle peak appeared ($2\theta = 2.3^o$) in all as-made samples indicated the formation of ordered structure in mesoporous scale [20]. The crystal structure of these samples that was investigated by wide angle XRD ($2\theta = 10–80^o$) showed a typical anatase TiO_2 phase with characteristic diffraction peaks at 2θ equal to 25.2, 38, 48, 54–55, 63 and 69–70 and 75–76° with traces of brookite phase at 30.8° [21]. The peaks that indexed as in order of increasing diffraction angles indicated a body centered tetragonal crystalline structure of TiO_2 crystal. The XRD spectra of Fig. 1b show weakness of the peaks as going from A to B and from C to D samples as well as vanishing of some others as in spectrum D; reflecting the poor crystallization and the amorphism of this sample devoted from SDS. The mean fraction of brookite (X_B) in the crystal lattice is calculated based on the relationship between the integrated intensities of anatase (1 0 1) and brookite (1 2 1) peaks by the following formula [22]; $X_B = 1/1 + K(I_A/I_B)$ where I_A, I_B are the integrated intensities of anatase, brookite peaks, respectively. The empirical constant K was determined via an XRD analysis of powders of known proportions of pure anatase and pure brookite TiO_2, and is equal to 2.72. The mass fraction of brookite varies from 5% in sample A reaching 15% in sample C. The XDR of sample D showed a very bad crystallinity therefore calculations related with size or with the anatase/brookite relative abundance can hardly be measured.

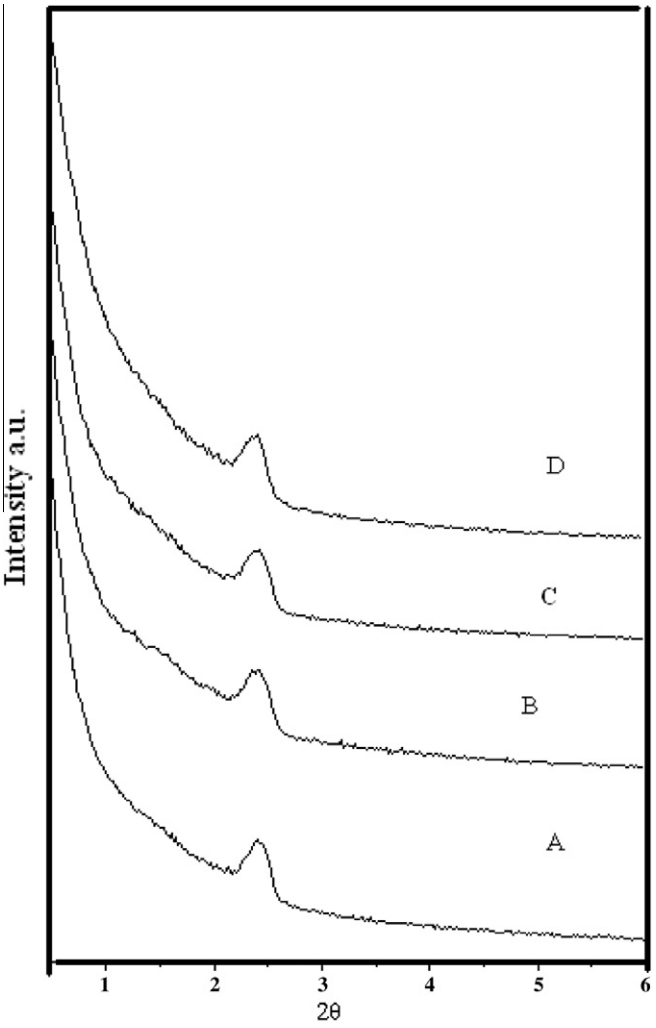

Fig. 1a. Low angle XRD patterns of silver containing titania samples where (A) 1.6 wt.% Ag/TiO_2 templated by POL (B) 3.2 wt.% Ag/TiO_2 templated by POL (C) 1.6 wt.% Ag/TiO_2 templated by SDS and (D) 3.2 wt.% Ag/TiO_2 templated by SDS.

Crystallite size was calculated from the anatase (1 0 1) reflection located at 25.4° using the Debye–Scherrer equation [23]. The particle sizes of anatase were around 30, 25 and 18.7 nm for the samples A, B and C, respectively. This shows the inhibition effect of increasing Ag content on the size growth of anatase nanoparticles; that has been depicted from increasing the samples amorphism with increasing Ag content. Since the main (1 1 1) crystal plane diffraction peak of Ag is located at almost the same position as (0 0 4) and (2 2 0) positioned, respectively at 38° and 43° peaks of anatase TiO_2, it is hard to distinguish these two peaks due to the broadening of the XRD patterns. However, increasing the intensity of peak; at 38°, form A to B as a result of increasing Ag content; rather than decreasing, let us presume that this peak is a result of silver peak overlapping. Superposing the plane of anatase at 38° with that of Ag^0 prohibit us to determine correctly the particles size of the latter. The peak intensity of titania crystals is reduced as a result of increasing the amount of silver ions that suffered reduction and thus their increased migration to the titania surface is indeed expected. On the other hand, a marked decrease in intensities of anatase structure is perceived for the sample assembled by SDS; however, the band at 38° was the only peak increased in intensity (in D sample); upon comparison with the C one, revolving its attribution to silver peak overlap.

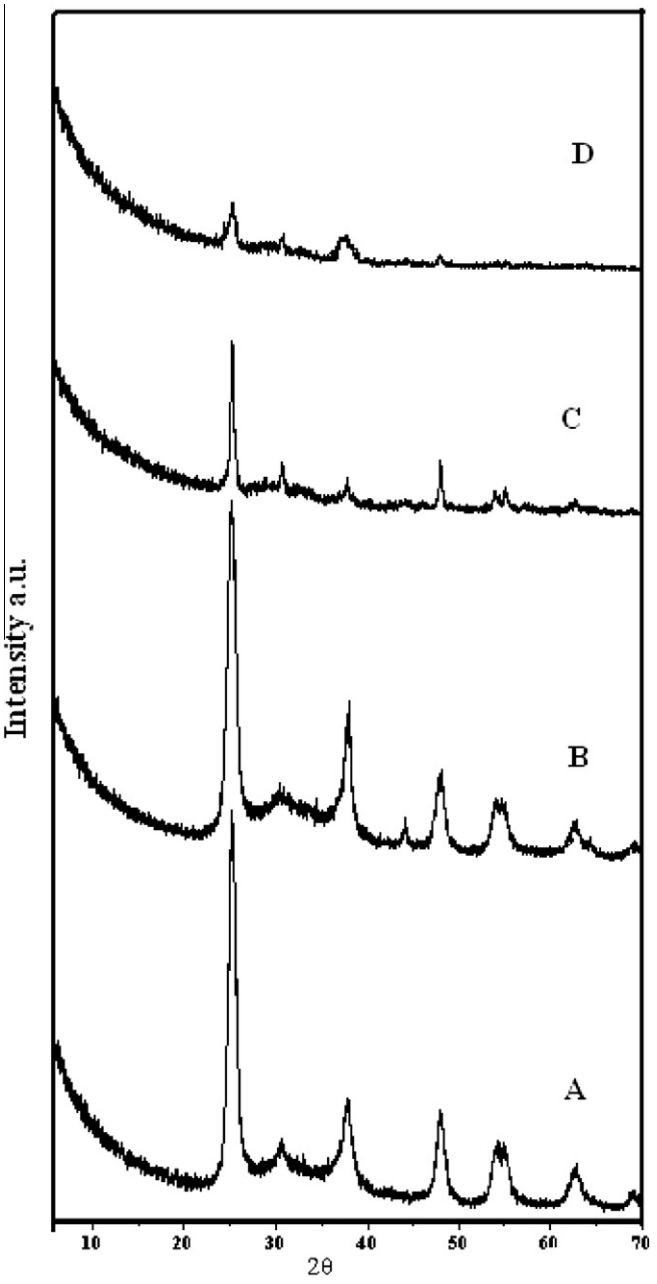

Fig. 1b. high angle XRD patterns of silver containing titania samples where A, B, C and D are typical to those mentioned in Fig. 1a.

3.2. Surface texturing

Fig. 2 shows the nitrogen adsorption–desorption isotherms of the as-synthesized samples. The adsorption isotherms show a type IV material through establishing steps on adsorption branches at P/P^o = 4–4.5. The isotherms also show hysteresis loops in the range of mesopores with a clear step in the isotherms [24]. For a type IV isotherm, one would expect that the volume adsorbed should become constant at high P/P^o. This does appear to be the case. This could lead us to interpret that these samples are mesoporous in nature.

The textural properties of all samples are given in Table 1. More emphasize into the pore type and its influence by Ag nanoparticles is imposed from V_t–t plot (Fig. 3). All samples show upward deviations confirming again the existence of mesopores. The BJH pore size distribution (not shown); derived from the isotherms shown in Fig. 2, presents a wide pore size emphasizing again the existence

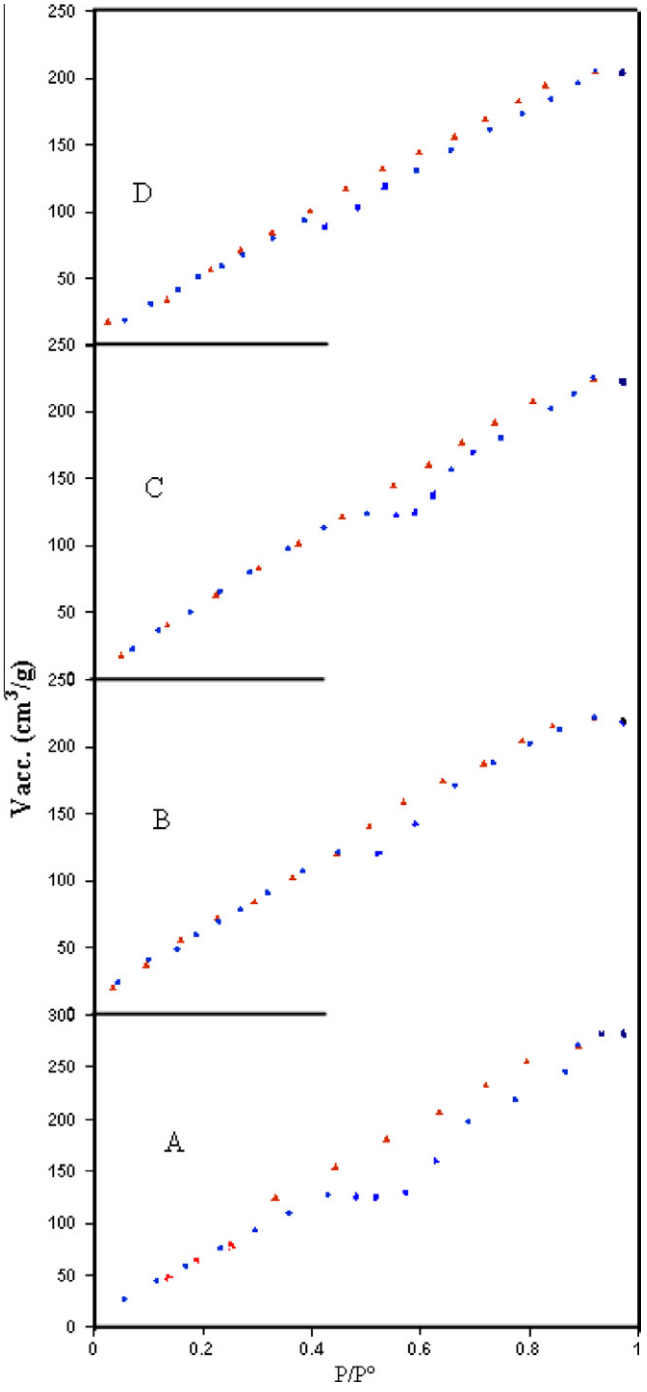

Fig. 2. N_2 adsorption isotherms of Ag titania catalysts where A, B, C and D are typical to those mentioned in Fig. 1a.

of mesostructure. The plots of A, C and D possessed a texture dominated by wider pores; in the 4.0–14.0 Å range; as assessed previously by hysteresis loops, than sample B; 4–11.0 Å. This indeed confirms the latter conclusion; concerning meso-structures, together with the isotherms (hysteresis loops) that predicts the wideness of the pore size distribution. The Ag content affects the specific surface area and thus causes a decrease from A; 390 m^2/g to B (333 m^2/g) as well as from C (412 m^2/g) to D (330 m^2/g) comprehending the incorporation of Ag atoms inside some of titania pores in both types of preparation. The pore radius of the samples follows a decrease from A to B but however showed a significant increase from C (22.7 Å) to D (25.0 Å). On the other hand, the pore volume decreased gradually from A to B and from C to D, emphasizing generally the incorporation of silver nanoparticles inside the pores of titania. Sample C gives the highest S_{BET} between all samples (412 m^2/g) since it indicates the lowest pore radius (22.7 Å) and also presents high enough pore volume as well (0.4677 cm^3/g). Although samples B and D gave the highest microporosity percentages, they exhibited the lowest S_{BET} values (see Table 1). This might indicate that the metal particles are located at the pore entrances completely blocking them. Increasing Ag content (3.2 wt.%) is indeed responsible for blocking some titania pores, irrespective of the template used, during the synthesis processes [25], as also emphasized from the decreased hysteresis loops of these samples (B and D when compared with A and C, respectively).

3.3. Ultraviolet–vis diffuse reflectance spectroscopy

Fig. 4 presents UV/vis diffuse reflectance spectra of the prepared materials. They exhibit new optical properties concerning about the absorption, which are different from those of TiO_2. The anatase showed sharp three absorption edges with the band gap absorption onset at 209, 283–286 and 395 nm for all samples. The latter absorption is associated to the $O^{2-} \rightarrow Ti^{4+}$ charge transfer corresponding to electronic excitation from the valence band to the conduction band. Samples C and D showed another single sharp edge with the band gap absorption onset at 346 nm. This may be generated due to the decrease in the amount of anatase concentration. As Ag^+ content increases, the absorbance in 200–360 nm region decreases; as noticed in B and D samples. Where at low Ag^+ content the dispersion of Ag on nano TiO_2 supports has significantly increased the ultraviolet and visible photoresponses of TiO_2, as depicted for A and C samples. At low percentage of Ag^+ (sample C), an absorption band, which extended up to 634 nm was depicted. An asymmetric but well-defined SPR bands appeared as an edge to absorb light with wavelength up to 700 nm in all samples; narrowing the band gap into ~1.8 eV [26]. These band gaps of Ag–TiO_2 are lower than that of the mother sample (3.14 eV) and thus, reflect the effect of Ag nanpoarticles on the main band edges of the titanium oxide. This suggests that nanosilver contributed to the red shift for the band gap narrowing, due to the occurrence of some electronic structure modification. This significant narrowing of the band gaps and the visible light absorbance of Ag/TiO_2 materials are of great importance for their practical applications since they could be active even by sunlight. The absorption curve of TiO_2 (not shown) indicates that TiO_2-only has no absorption in the spectral region above 420 nm [27]. Following encapsulation of Ag nanoparticles onto TiO_2, the absorption curves of (A–D) were obviously improved in the 380–780 nm spectral region. Such additional absorption peaks in the visible region occur because of the surface plasmon resonance (SPR) and the interference of electromagnetic field with the conduction electrons of silver nanoparticles dispersed on the TiO_2 support [28,29].

3.4. Fourier-transform infrared spectrometry

FT-IR spectra for Ag/TiO_2 catalysts calcined at 450 °C (Fig. 5) demonstrate a broad absorbance peak in the range from 3100 to 3500 cm^{-1} assigned to hydroxyls vibration and a strong absorbance peak around 1630 cm^{-1} attributed to the vibrations of the surface-adsorbed H_2O and Ti–OH bonds [27]. These FT-IR spectra show residual absorption peaks attributed to C–H stretching and bending modes, suggesting that the bulk of templates have not completely removed by calcination at 450 °C. Comparing the FT-IR spectra of the samples, the bands at low frequency (below 1000 cm^{-1}) attributed to Ti–O–Ti vibrations in TiO_2 [30] change with Ag incorporation especially the band in the margin 450–

Table 1
Surface texturing data of Ag titania catalysts.

Sample	S_{BET} (m^2/g)	S_t (m^2/g)	V_p^{total} (cm^3/g)	V_p^{μ} (cm^3/g)	$V_p^{wid.}$ (cm^3/g)	S^{ext} (m^2/g)	S^{μ} (m^2/g)	S^{wid} (m^2/g)	r^- (Å)	Microporosity (%)	C
A (1.6 wt.% Ag/TiO_2 from POL)	390	432	0.5425	0.3422	0.2003	143.3	213.5	176.4	27.0	54.75	26.4
B (3.2 wt.% Ag/TiO_2 from POL)	333	387	0.4407	0.4127	0.0280	19.8	305.6	27.3	26.4	91.79	28.1
C (1.6 wt.% Ag/TiO_2 from SDS)	412	372	0.4677	0.3815	0.0862	43.9	315.4	96.5	22.7	76.55	23.8
D (3.2 wt.% Ag/TiO_2 from SDS)	330	341	0.4129	0.3569	0.0560	39.5	271.02	58.9	25.0	82.12	25.1

Note: BET-surface area (S_{BET}), total pore volume (V_p), mean pore radius (r^-), surface area derived from V_l–t plots (S_t), surface area of micropores (S^{μ}), external surface area (S^{ext}), surface area of wide pores (S^{wid}), volume of micropores (V_p^{μ}), volume of wide pores ($V_p^{wid.}$) and microporosity percentages $V_p^{mic}/V_p^{total} \times 100$.

500 cm^{-1} for A and B. The non influence of the band at 550 cm^{-1} for C and D samples upon Ag incorporation predicts the limited effect of Ag on the skeletal vibration of TiO_2 upon using SDS as template. The adsorbed water and hydroxyl groups are crucial to the photocatalytic reactions since they react with photoexicited holes on the catalyst surface to produce hydroxyl radicals, as powerful oxidant. Obviously, the intensity of the bands in A, B and C is much stronger; i.e. susceptible to generate higher electron–hole pairs, than that of D, indicating that the introduction of Ag by this method (SDS surfactant) at high Ag content make the sample possesses less surface-adsorbed hydroxyl groups or water.

3.5. Transmission electron microscopy

TEM images of Ag (0.1)/TiO_2 (A) and Ag (0.2)/TiO_2 (B); those derived from POL, are shown in Figs. 6a and 6b. Titania nanodomain arrays are observed in the TEM images where Ag nanoparticles are seen as small black dots (core) embedded into larger spherical TiO_2 material (shell), which are lighter. The spherical titania particles were found to be in the range of 15–25 nm for sample A and 11–16 nm for sample B in line with the one depicted by XRD measurements. It is observed from TEM image in Fig. 6a, that the particle size of the sample have a strong inclination to aggregate, indicating they have very high unsaturated surface energy. However, that aggregation tendency seems to disappear in image B comprehending a change in surface property.

The micrographs of these catalysts (A and B) show that the silver particles are highly dispersed on the surface of TiO_2 in both samples indicating average particle size of 7 nm; for A sample, and 5 nm for B sample. The micrograph of the samples synthesized by deposition–precipitation employing SDS surfactant (C and D – not shown) indicates typical morphological characteristics of A and B however, Ag nanoparticles size are found to be lower exhibiting diameter comprised of 5 and 3 nm, respectively. The uniform distribution of nano particles and small particles size indicates the efficiency of the present preparation methods. The smaller size for the particles could be attributed to an increase in the thermal stability and the resistance to sintering [11]. This indicates the effectiveness of template assembly methods for mesoporous titania preparation adopted in this study. Decreasing the grain size of anatase upon increasing Ag doping from 1.6 to 3.2 wt.% comprehend the inhibition effect of metallic Ag on crytallites size of titania.

3.6. Photocatalytic activity

Firstly, a blank run was performed, using photolysis, which showed negligible herbicide degradation (<4% after 15 h). Titania with varying Ag nanoparticles was used to oxidize the herbicide solution and the different performances are shown in Fig. 7. The samples prepared by polyoxyethylene laurel ether showed higher photocatalytic activities than the ones synthesized using SDS, probably due to the higher crystallinity and higher anatase content, depicted from XRD measurements. The P25 sample presented activity comparable to that of the C sample but indeed lower than those of A and B ones. At the beginning, most possibly the contri-

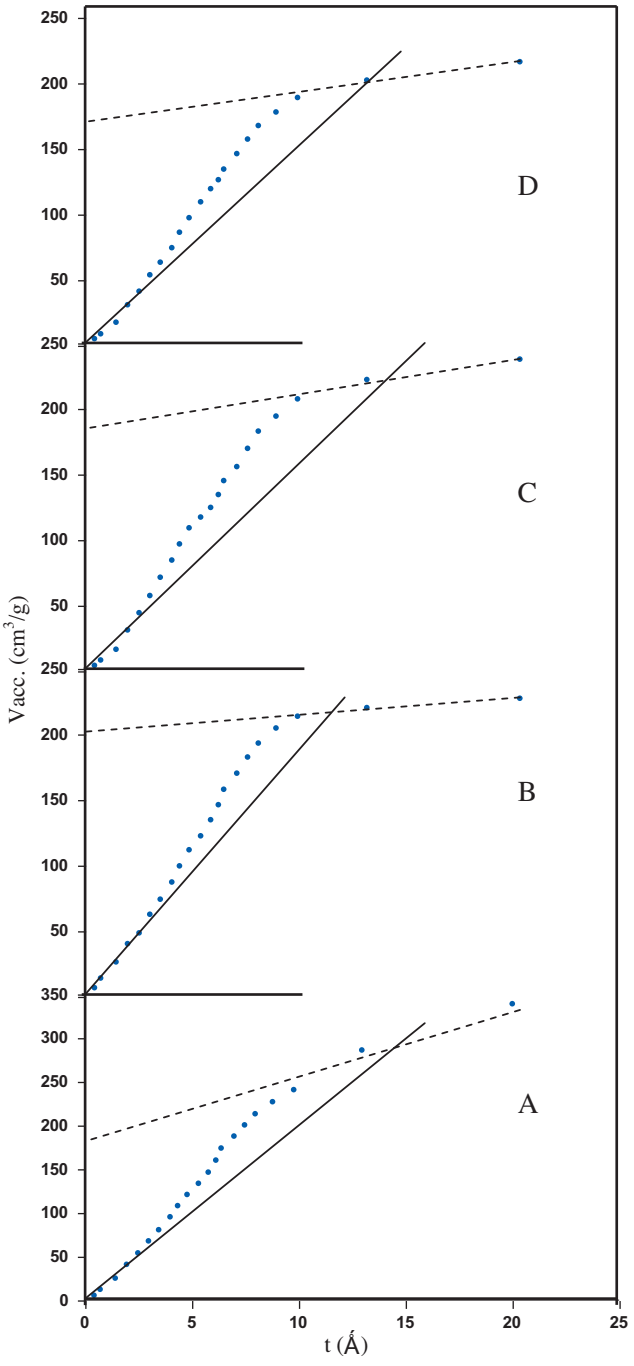

Fig. 3. V_l–t plot of Ag titania catalysts where A, B, C and D are typical to those mentioned in Fig. 1a.

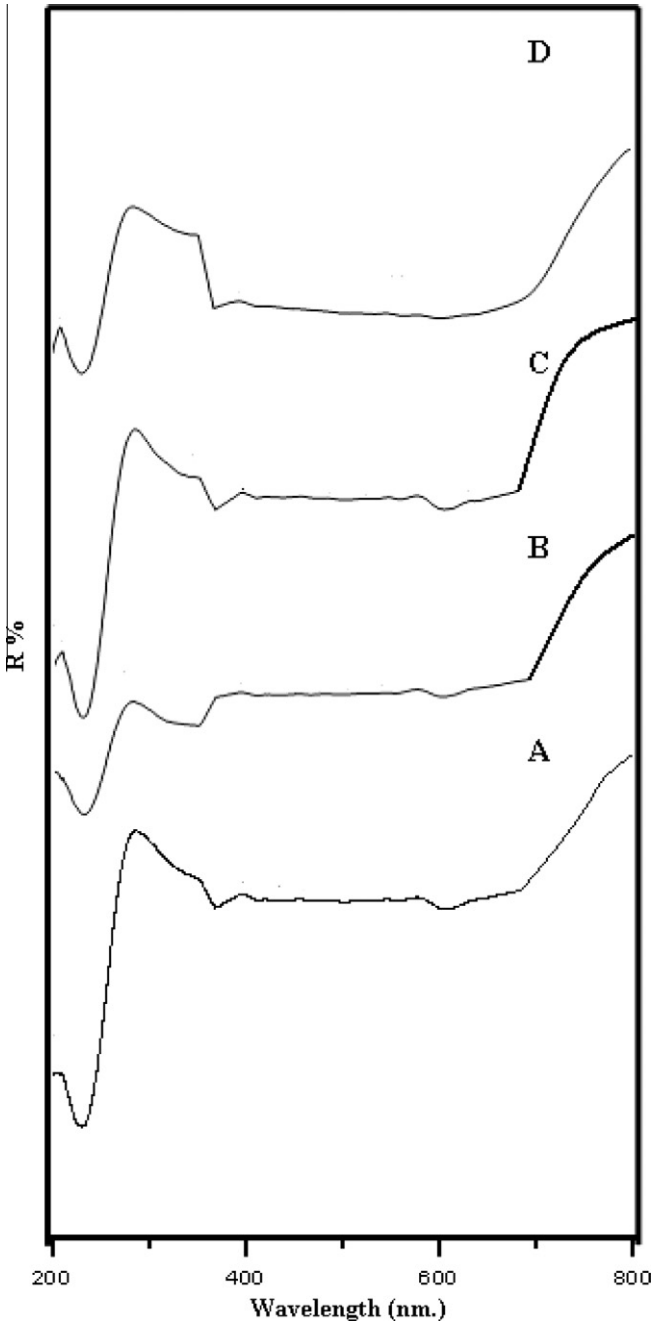

Fig. 4. UV–vis spectra of Ag titania catalysts where A, B, C and D are typical to those mentioned in Fig. 1a.

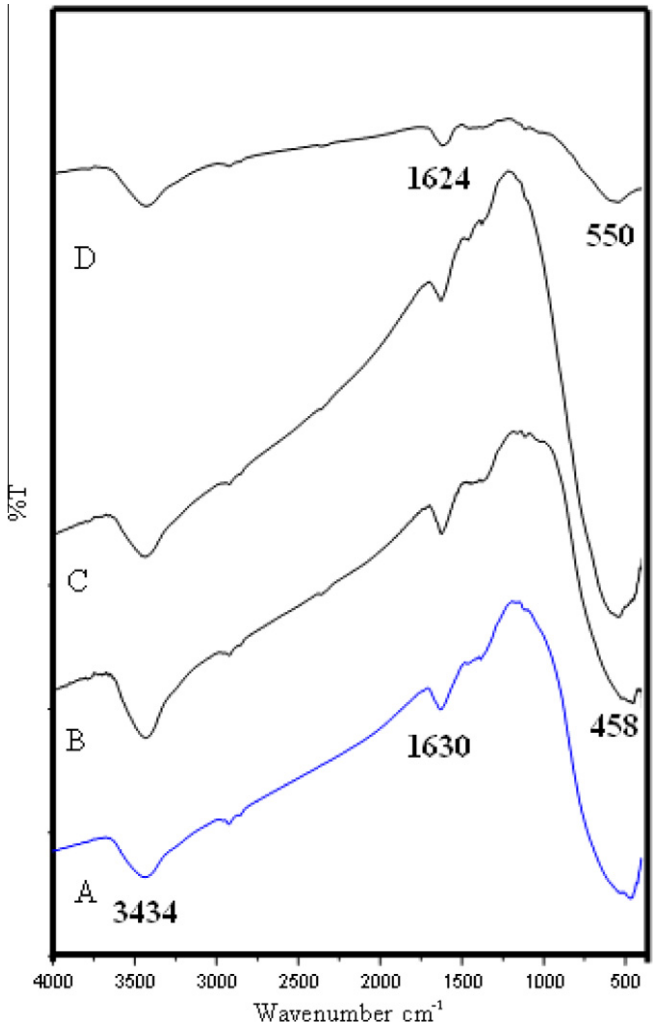

Fig. 5. FT-IR spectra of calcined Ag/TiO_2 samples where A, B, C and D are typical to those mentioned in Fig. 1a.

bution of herbicide adsorption is favored by the larger mesopore volume, pore radius and surface areas of our synthesized samples (Table 1). Metal oxide nanoparticles (especially TiO_2) are known to catalyze oxidation reactions by photo-induction and thus require UV–vis light irradiation. In this work, the type of catalysis was investigated by repeating the experiment under visible-light illumination. The reaction rates are not similar under both light of illumination. After 140 min, degradation of 95% for sample A under UV illumination was achieved where it reached 82%, 38%, 38% and 27% for samples B, C, P25 and D, respectively (Fig. 7). With visible-light illumination the samples A, B, C and D achieved degradation equal 78, 70, 50 and 38%, respectively (Fig. 8). P25 Degussa presented very low activity comprised of 5% degradation exhibiting limited amount of holes, comparatively (Fig. 8). Although the titania P25 (Degussa) has shown promising photocatalytic activity compared with other TiO_2 materials [31] because of increased charge separation efficiency in interfacial electron transfer between anatase and rutile phases [32], P25 presents low activity probably for increasing its energy gap to be effective under visible-light illumination.

The photocatalytic degradation of 2,4-D as a function of the irradiation time was observed to follow an exponential decay like form as depicted in Figs. 7 and 8. Besides, a plot of $\ln(C_0/C)$ versus time for the herbicide in the optimized conditions under visible-light illumination was also linear (Fig. 9), suggesting that the photodegradation reaction follows the pseudo-first-order reaction kinetics. The pseudo first-order reaction rate constant calculated for the four catalysts under visible-light illumination were 0.0335 min^{-1} (A), 0.0289 (B), 0.0263 (C), and 0.0251 min^{-1} (D). Thus, vis/Ag–TiO_2 catalyst derived from polyoxyethylene laurel ether was found to be a very effective to degrade the model pollutant in aqueous solution. Discrepancy between the pseudo-first-order reaction rate constants may be due to different photocatalytic degradation mechanisms and/or owing to a competition for degradation between the reactant and the intermediate products.

Afterward, the photocatalytic activities decreased with increasing Ag content stating that the photocatalytic activity for A was marginally better than rest of samples as given in the above order. This can be explained in view of the characterization of the inves-

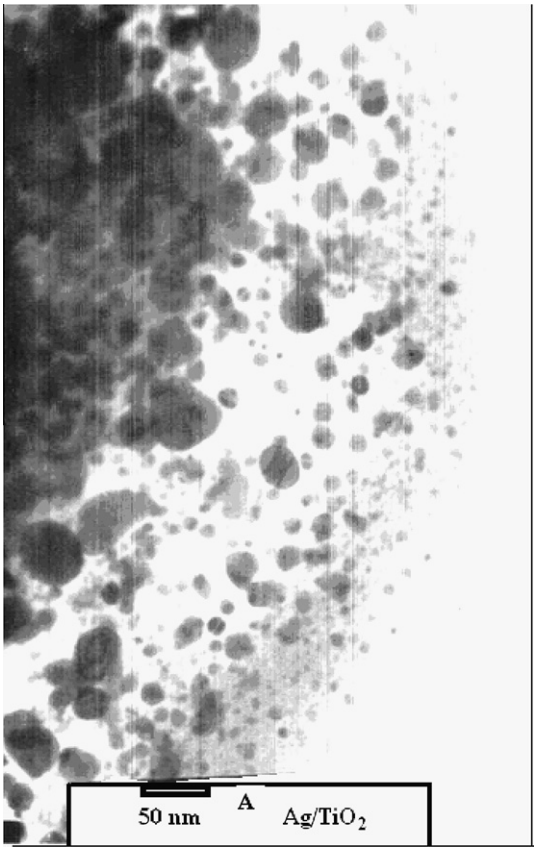

Fig. 6a. TEM image of Ag/TiO_2 at a loading of 1.6 wt.% derived from the POL template.

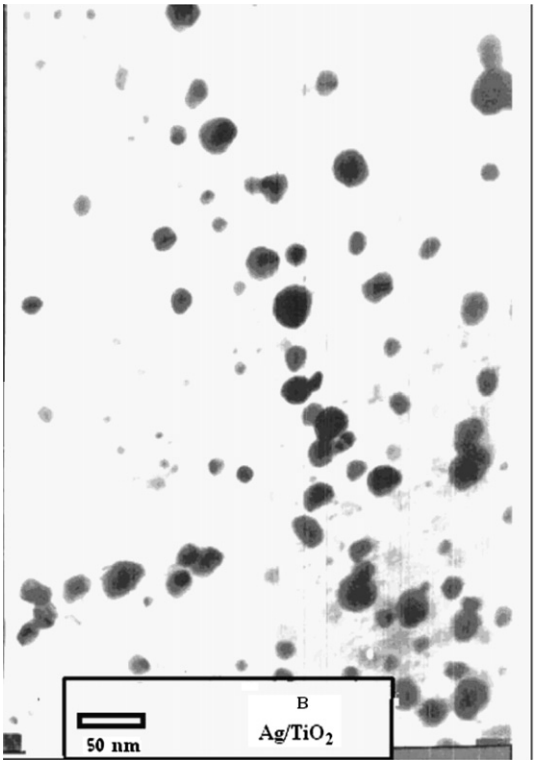

Fig. 6b. TEM image of Ag/TiO_2 at a loading of 3.2 wt.% derived from the POL template.

tigated Ag/TiO_2 materials. It can state that not only the surface area plays an important role on the photocatalytic activity but also the crystallinity of the base TiO_2 of acceptable nanosize. On the other hand, nanosized materials have shown abundant defects; as in the D sample, due to their poor crystallinities. These defects are acted as recombination centers for photogenerated holes and electrons, thus affecting their photocatalytic efficiencies [33]. The fact that D had the lowest photocatalytic activity among all samples is consistent with the observation from XRD, where D had the lowest crystallinity although it shows the lowest TiO_2 particles size comparatively. If the particle size effect is the dominant factor for the photocatalytic activity, the sequence of D > C > B > A could have been obtained for the activity. This was opposite to the experimental observation as the photocatalytic activity order was reversed being A > B > C > D. This conflict suggested that the size variable was not the determining factor. The dominant factor responsible for the photocatalytic activity order of A > B > C > D may be the formation of Schottky barriers between TiO_2 and Ag^0. It is acknowledged that the radius of the Ag^+ and Ag atom is much larger than the Ti^{4+}, so very unlikely for Ag^+ and Ag atom to enter the TiO_2 lattice [34]. In fact, the Ag atoms were in direct contact with the TiO_2 nanoparticles. Because the work function of the metal Ag is higher than that of TiO_2, electrons are removed from the TiO_2 particles to the vicinity of the Ag particles. This results in the formation of Schottky barriers at the Ag–TiO_2 contact region and results in charge separation [35] i.e. the electronic interaction occurring at the contact region between the metal deposits and the semiconductor surface [36]. The Ag deposits act as electron traps immobilizing the photogenerated electrons in the traps and shortly transferring them to oxygen to form highly oxidative species such as O_2^-. This type of electron scavenging by Ag metal is reported to be a faster process compared to the electron transfer to oxygen (or) recombination with holes [36] since, the trapping of electron by Ag metal from TiO_2 occurs at a faster rate when compared to the electron transfer from TiO_2 to O_2 [37,38].

More specifically, Schottky barriers facilitate the electron transfer from TiO_2 nanoparticles (with high Fermi level) to Ag (with low Fermi level), resulting in higher transferring efficiency of electrons [39]. The effect of Schottky barriers in our particular case was evidenced by the fact that all the Ag-loaded TiO_2 had higher photocatalytic efficiencies than Ag free TiO_2. Firstly, the Schottky barriers facilitate the photoelectron movement to a certain direction, from the semiconductor TiO_2 nanoparticles to adjacent Ag atom or cluster. Sample A has the highest photocatalytic activity and can be attributed to the fact that Ag was distributed at surface of the

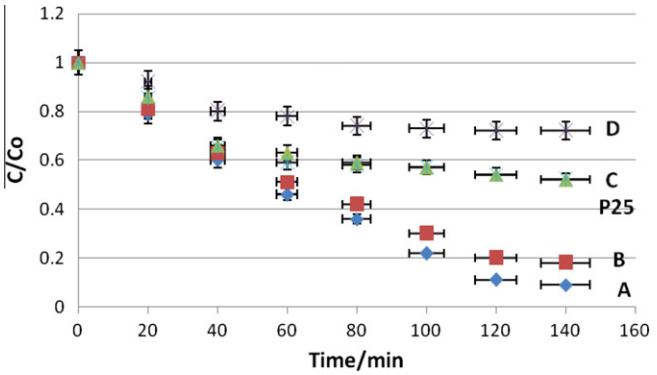

Fig. 7. Plot of the relative concentration of 2,4-dichlorophenoxy acetic acid (C/C_0, where C_0 = 50 mg/l, 100 ml) vs ultraviolet irradiation time in the presence of Ag/TiO_2 photocatalysts (1.5 g/l) templated from polyoxyethylene laurel ether (A = 1.6 wt.% Ag/TiO_2 and B = 3.2 wt.% Ag/TiO_2) and sodium dodecylsulphate (C = 1.6 wt.% Ag/TiO_2 and D = 3.2 wt.% Ag/TiO_2) in comparison with P25.

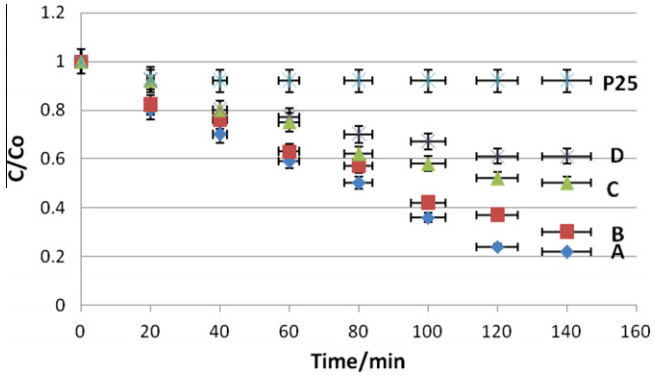

Fig. 8. Plot of the relative concentration of 2,4-dichlorophenoxy acetic acid (C/C_0, where C_0 = 50 mg/l, 100 ml) vs visible-light irradiation ($\lambda \geqslant 420$ nm) time in the presence of Ag/TiO_2 photocatalysts (1.5 g/l) templated from polyoxyethylene laurel ether (A = 1.6 wt.% Ag/TiO_2, B = 3.2 wt.% Ag/TiO_2) and sodium dodecylsulphate (C = 1.6 wt.% Ag/TiO_2 and D = 3.2 wt.% Ag/TiO_2) in comparison with TiO_2 Degussa.

TiO_2. For this sample, the Schottky barriers attract the electrons and the holes will be left on the surface layer of the TiO_2. This attraction greatly inhibits the recombination of electron–hole pairs. The enriched holes in the surface layer can directly degrade herbicide, at the same time, it can oxidize H_2O adsorbed on the surface and produce hydroxyl radicals ($OH^{\cdot}$) that can degrade organic matters effectively. Secondly, the most efficient UV illumination was achieved on the A sample because there was the lowest amount of Ag on the TiO_2 surface. Increasing the Ag particles concentration on the top of TiO_2 surface block the UV light thus affecting the photocatalytic activity. Too much Ag loading content may result in a photohole trapping effect [40]. This trapping effect was negligible when the Ag concentration equal 1.6 wt.% and the Schottky barrier predominantly promoted the TiO_2 charge separation efficiency. With increasing Ag content beyond 1.6 wt.%, the trapping effect became prevailing and the photocatalytic activity declined. The decline in the photocatalytic activity can also be associated with the change of the reaction site density.

On the other hand, the Visible light degradation of 2,4-dichlorophenoxyacetic acid on samples C and D was faster than under UV light for same samples possibly due to a contribution from direct or homogeneous photolysis and/or due to the residual sulphate might be remained in the catalysts following the synthesis using SDS [41]. Accordingly, the exhibited increase in the sample C absorption bands as well as the plasmon resonance absorbance around 700 nm for both C and D samples might contribute in promoting visible light adsorption [40] as well. The residual carbon depicted

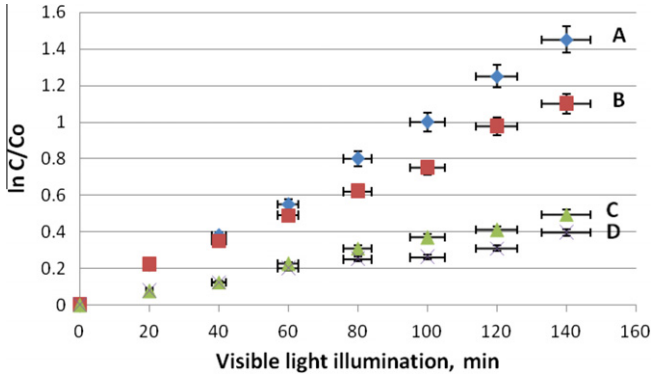

Fig. 9. A plot of $\ln C_0/C$ vs visible-light illumination time from Ag/TiO_2 photocatalysts (1.5 g/l) templated from polyoxyethylene laurel ether; (A = 1.6 wt.% Ag/TiO_2 and B = 3.2 wt.% Ag/TiO_2) and sodium dodecylsulphate (C = 1.6 wt.% Ag/TiO_2 and D = 3.2 wt.% Ag/TiO_2).

Table 2
Effect of catalyst recycling on rate constant (k, min^{-1}).

Catalyst name: Ag/TiO_2 derived from polyoxyethylene laurel ether (A)	Visible-light illumination extends for 5 h
Ist cycle	0.0335
2nd cycle	0.0301
Third cycle	0.0252

from IR result could also share on the visible light absorption and consequently the activity.

More adsorption of 2,4-D enhances the transfer of photoexcited electron from the visible light sensitized 2,4-$D^{\cdot}$ to the conduction band of TiO_2 [42]. Sequentially, electron transfer to oxygen occurs via Ag-traps. In addition, the rate-determining step in photo-catalytic oxidation is believed to be the electron transfer from Ag/TiO_2 surface to the adsorbed oxygen [43]. Thus, the 2,4-D adsorption as well as charge separation becomes vital for the photodegradation under visible-light irradiation whereas under UV irradiation, sensitization of TiO_2 takes place.

In order to test the efficiency of used Ag/TiO_2 (A) catalyst, experiments were carried out with 1×10^{-4} M concentration of herbicide with a catalyst loading of 1.5 g L^{-1} of the herbicide solution under visible-light irradiations. After the completion of the degradation, the Ag/TiO_2 catalyst at the end of the I cycle was collected and utilized for the II and III cycles for the same initial concentration of herbicide. The first order rate constants of reactions using I, II and III recycled Ag/TiO_2 are given in Table 2. The decrease in activity of Ag/TiO_2 is not to a greater extent even at the end of III cycle under visible light for the illumination period of 5 h. Such high photonic stabilities and efficiencies of the mesoporous Ag/TiO_2 catalysts can be attributed to a lower light scattering effect of the ordered mesoporous TiO_2 material [44,45].

4. Conclusion

In summary, the nano Ag/TiO_2 photocatalysts derived from POL exhibit much higher efficiency for the photodegradation of the herbicide pollutant than those derived from SDS under UV and visible-light irradiations due to the higher efficiency of generation and separation of photoinduced electrons and holes in the former than those in the latter. The sequence of the photocatalytic activity was A > B > C > D, which was explained systematically using the Schottky barrier, the photohole trapping effect and the reactive reaction site density. As a second priority, the photocataltyic activity dependence was respectively correlated to crystallinity and surface area (adsorption). The defects obtained as a result of decreased crystallinity influenced photocatalytic efficiencies since it acts as recombination centers of photogenerated holes and electrons. Besides, the formation of brookite phase that is catalyzed by increasing the Ag^{+} concentration at the expense of anatase phase affected photoresponses of Ag/TiO_2 catalysts. At 1.6 wt.% Ag, the dispersion of Ag; at appropriate diameter of 7 nm, on nano titania has significantly increased UV and vis photoresponses of TiO_2 resulting increase of their photocatalytic efficiencies together with their high unsaturated surface energies as depicted from TEM investigations. Considering the larger internal surface area of all samples, most of anatase phase exists as nanoparticulates bricks forming the pore walls. Hence, the photocatalytic $OH^{\cdot}$ radical might migrate into TiO_2 external surfaces activating the herbicide oxidation.

Acknowledgment

This work was supported by Basic Research Program of the Institute of Scientific Research and Revival of Islamic Heritage, Umm Al-Qura University, Saudi Arabia.

References

[1] M.A. Fox, Acc. Chem. Res. 16 (1983) 314;
M.A. Fox, M.T. Dulay, Chem. Rev. 93 (1993) 341–349.
[2] P.V. Kamat, J. Phys. Chem. C 111 (2007) 2834;
P.V. Kamat, Chem. Rev. 93 (1993) 267–273.
[3] A.J. Bard, M.A. Fox, Acc. Chem. Res. 28 (1995) 141–149.
[4] M.M. Mohamed, W.A. Bayoumy, M. Khairy, Micropor. Mesopor. Mater. 109 (1–3) (2008) 445–457.
[5] M.M. Mohamed, I. Othman, R.M. Mohamed, J. Photochem. Photobiol. A 191 (2–3) (2007) 153–161.
[6] M.M. Mohamed, T.M. Salama, I. Othman, J. Mol. Catal. 273 (2007) 189–198;
M.M. Mohamed, W.A. Bayoumy, M. Khairy, M.A. Mousa, Micropor. Mesopor. Mater. 97 (2006) 66–77.
[7] S.M. Zakeeruddin, Md.K. Nazeeruddin, R. Humphry-Baker, P. Pechy, P. Quagliotto, C. Barolo, G. Viscardi, M. Gratzel, Langmuir 18 (2002) 952–959.
[8] S. Burnside, J.E. Moser, K. Brooks, M. Gratzel, D. Cahen, J. Phys. Chem. B 103 (1999) 9328–9336.
[9] S.H. Elder, Y. Gao, X. Li, J. Liu, D.E. McCready, C.F. Windisch Jr., Chem. Mater. 10 (1998) 3140–3146.
[10] W. Mu, J.M. Herrmann, P. Pichat, Catal. Lett. 3 (1999) 73–79.
[11] K.E. Karakitsou, X.E. Verykios, J. Phys. Chem. 97 (1993) 1184–1192.
[12] Y. Zang, R. Farnood, Appl. Catal., B 79 (2008) 334–343.
[13] N. Kakuka, N. Goto, H. Ohkita, T. Mizushima, J. Phys. Chem. B 103 (1999) 5917–5925.
[14] S. Rodrigues, S. Uma, I.N. Martyanov, K.J. Klabunde, J. Catal. 233 (2005) 231–239.
[15] E.C.H. Sykes, F.J. Williams, M.S. Tikhov, R.M. Lambert, J. Phys. Chem. B 106 (2002) 5390–5397.
[16] X.Z. Li, F.B. Li, Environ. Sci. Technol. 35 (2001) 2381–2389.
[17] L. Lhomme, S. Brosillon, D. Wolbert, J. Photochem. Photobiol. A 188 (2007) 34–41.
[18] S. Malato, J. Blanco, A. Vidal, Appl. Catal., B 37 (1) (2002) 1–8.
[19] N. Watanabe, S. Horikoshi, A. Kawasaki, H. Hidaka, Environ. Sci. Technol. 39 (7) (2005) 2320–2326.
[20] H. Luo, C. Wang, Y. Yan, Chem. Mater. 15 (2003) 3841–3847.
[21] JCPDS PDF-2 Pattern 01-076-1935.
[22] R. Spurr, H. Myers, Anal. Chem. 29 (1957) 760–764.
[23] B.D. Cullity, Elements of X-ray Diffraction, Addison-Wesley Publishing Company Inc., London, 1978. p. 99.
[24] I. Othman, R.M. Mohamed, I.A. Ibrahiem, M.M. Mohamed, Appl. Catal., A 299 (2006) 95–102.
[25] M.M. Mohamed, F.I. Zidan, M. Thabet, Micropor. Mesopor. Mater. 108 (2008) 193–203.
[26] K.H. Hong, J.L. Park, I.H. Sul, J.H. Youk, J. Kang, J. Polym. Sci. Part B: Polym. Phys. 44 (2006) 2468–2477.
[27] Y. Liu, X. Wang, F. Yang, X. Yang, Micropor. Mesopor. Mater. 114 (2008) 431–439.
[28] D. Long, W. Qiao, L. Zhan, X. Liang, L. Ling, Micropor. Mesopor. Mater. 121 (2009) 58–59.
[29] M.M. Mohamed, M.M. Al-Esaimi, J. Mol. Catal. A: Chem. 255 (2006) 53–61.
[30] M. Burgos, M. Langlet, Sol–Gel Sci. Technol. 16 (1999) 267–275.
[31] W. Li, C. Liu, Y. Zhou, Y. Bai, X. Feng, Z. Yang, L. Lu, X. Lu, K.-Y. Chan, J. Phys. Chem. C 112 (2008) 20539–20545.
[32] T. Tachikawa, S. Tojo, M. Fujitsuka, T. Majima, Chem. Eur. J. 12 (2006) 3124–3137.
[33] Y. Li, W. Xie, X. Hu, Langmuir 26 (1) (2010) 591–597.
[34] K.V.S. Rao, B. Lavedrine, P. Boule, J. Photochem. Photobiol. A 154 (2003) 189–195.
[35] K. Awazu, M. Fusimaki, C. Rockstuhp, J. Tominaga, H. Murakami, Y. Onki, N. Yoshida, J. Am. Chem. Soc. 130 (5) (2008) 1676–1683.
[36] J.A. Rengifo-Herrera, K. Pierzchała, A. Sienkiewicz, L. Forro, J. Kiwi, C. Pulgarin, Appl. Catal., B 88 (2009) 398–406.
[37] Z. Cheng, Y. Li, Chem. Rev. 107 (2007) 748.
[38] J.M. Gole, J.D. Stout, C. Burda, Y. Lou, X. Chen, J. Phys. Chem. B 108 (2004) 1230–1237.
[39] S. Sen, S. Mahanty, S. Roy, O. Heintz, S. Bourgeois, D. Chaumont, Thin Solid Films 474 (2005) 245–253.
[40] T. Hirakawa, P.V. Kamat, J. Am. Chem. Soc. 127 (2005) 3928–3933.
[41] N. Fu, Y. Wu, Z. Jin, G. Lu, Langmuir 26 (1) (2010) 447–452.
[42] C. Hu, Y. Lan, J. Qu, X. Hu, A. Wang, J. Phys. Chem. C 110 (9) (2006) 4066–4072.
[43] S. Yoriya, C.A. Grimes, Langmuir 26 (1) (2010) 417–422.
[44] C. Li, M.Z. Hoffman, J. Phys. Chem. A 104 (2000) 5998–6005.
[45] A.A. Ismail, D.W. Bahnemann, L. Robben, V. Yarovyi, M. Wark, Chem. Mater. 22 (2010) 108–116.